Reactive Power Control of DFIG Wind Power System Connected to IEEE 14 Bus Distribution Network

Moayed Moghbel, Hasmina Tari Mokui , Mohammad A.S. Masoum, Mansour Mohseni

Department of Electrical and Computer Engineering, Curtin University, Perth, WA, Australia.

moayed.moghbel@postgrad.curtin.edu.au; h.mokui@postgrad.curtin.edu.au, m.masoum@curtin.edu.au, mansour. mohseni@curtin.edu.au

***Abstract*- With the increasing penetration of distributed wind turbines (WTs) in distribution systems, utilities are requiring these renewable resources to provide reactive power supports during steady-state and transient operating conditions. WTs with doubly fed induction generators (DFIGs) are able to independently control active and reactive power. The reactive power capability is subjected to several limitations resulting from the voltage, current, and speed, which changes with the operating point. This paper examines the reactive power control capability of DFIG-based WT by connecting it to the IEEE 14 bus distribution system. The stator-flux-oriented vector control principle is applied to build a model of the DFIG in dq synchronous coordination system, and the PSCAD/EMTDC simulation software is employed to investigate its performance in providing reactive power support to the grid.**

Index Terms: DFIG, reactive power support, Hysteresis current control, PWM voltage-source inverter, and IEEE 14 bus system.

I. INTRODUCTION

The installed wind power generation capacity around the world has significantly increased in the last decade and exceeded to about 159.2 GW in 2009. In particular, the installed wind turbine capacity in Australian power systems reached to 1.8 GW by the end of 2009; with further 10.2 GW projects currently in either development or evaluation stages [1]. Statistics show that doubly fed induction generators (DFIG) are the most employed technology for wind energy applications since 2002 [2]. DFIG has a number of advantages compared to fixed-speed generators including decoupled control of active and reactive power, improved power quality, and reduced mechanical stress. Moreover, DFIG is more economically viable than full-inverter variable-speed generators as it utilizes a relatively small voltage-source inverter (VSI) rated at about 30%–35% of the generator rating for a given rotor speed variation range of ± 25% [3], [4].

Fig. 1 shows the schematic diagram of DFIG-based wind generators. It consists of a wound-rotor induction machine (WRIM) which is mechanically coupled to the wind turbine through a shaft and gear-box system. For the WRIM, three-phase stator winding is directly connected to the coupling transformer while the rotor winding is connected through a back-to-back partial scale VSI. The system controllability is achieved through regulating current in the rotor side Converter (RSC) and grid side converter (GSC) which are connected through a DC-link capacitor.

The current controller of three-phase voltage-source inverters (VSI) is an essential part in the overall control structure of many applications, such as active power filters, ac motor drives, and uninterruptible power supplies [5]. The quality of the applied current controller greatly influences the overall control system performance. Therefore, over the past few decades, considerable research has been done on current control techniques, and from this work three major classes of current controller have evolved: predictive controllers, linear proportional–integral (PI) controllers, and hysteresis controllers [5], [6]. Predictive controllers are the most complex method and require the knowledge of load parameters. Extensive hardware implementation is another disadvantage of this technique. Linear PI current controller can limit the switching frequency of the inverter and produce a well-defined harmonic content. However, parameters of PI controllers must be carefully tuned with a trade-off between maintaining the system stability over the whole operation range and achieving an adequate dynamic response during transients. This can result in degraded transient performance, which in turn, hinders the application of PI current controller in high-demanding situations, such as active power filters [5]–[7]. Finally, hysteresis current controllers (HCC) have been widely used because of the noncomplex implementation, outstanding stability, absence of any tracking error, very fast transient response, inherent limited maximum current, and intrinsic robustness to load parameters variations [5], [6], [8]. Different control strategies have been proposed in the literature for voltage, frequency, active and reactive power control of DFIG systems [9].

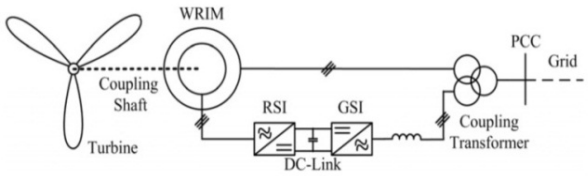

Figure 1. DFIG system

This paper implements a dynamic DFIG-based wind turbine model based on vector control strategy which includes hysteresis method control for rotor side converter and voltage source control for grid side converter. The model is implemented in PSCAD/EMTDC and included in the IEEE 14 bus distribution system to investigate its capability in providing reactive power support and improving the system voltage profile.

II. DFIG System Modeling

Field-oriented vector control, using rotational transformations, and linear proportional-integral (PI) controllers, has so far proved to be the most popular technique used in DFIG-based wind turbines [10]–[11]. In this double-closed-loop approach, the outer power control loop is employed to attain an independent control over the active and reactive powers of the machine. Synchronous-frame PI current controllers are then used in cascade with the outer control loop to regulate the rotor output current. The phase angle of the stator-flux space vector is usually used in the literature for the controller synchronization, estimated through an open-loop observer [11]–[12].

Fig. 2 shows the Γ-form equivalent circuit of the machine used in this paper for the machine modeling [13], [14]. The stator and rotor voltage and flux vectors in the arbitrary reference frame are defined as:

$$\mathbf{V}_s = R_s\mathbf{I}_s + \frac{d\boldsymbol{\lambda}_s}{dt} + j\omega\cdot\boldsymbol{\lambda}_s \tag{1}$$

$$\mathbf{V}_r = R_r\mathbf{I}_r + \frac{d\boldsymbol{\lambda}_r}{dt} + j(\omega-\omega_r)\cdot\boldsymbol{\lambda}_r \tag{2}$$

$$\boldsymbol{\lambda}_s = L_m(\mathbf{I}_s+\mathbf{I}_r) = L_m\mathbf{I}_m \tag{3}$$

$$\boldsymbol{\lambda}_r = L_\sigma\mathbf{I}_r + L_m(\mathbf{I}_s+\mathbf{I}_r) \tag{4}$$

where subscripts s and r denote stator and rotor parameters, ω is the angular speed of the arbitrary frame, L_m and L_σ are the magnetizing and leakage inductances, respectively. By using Eqs. 1-4, the stator current, rotor flux and voltage vectors can be expressed as

$$\mathbf{I}_s = \frac{\boldsymbol{\lambda}_s}{L_m} - \mathbf{I}_r \tag{5}$$

$$\boldsymbol{\lambda}_r = \boldsymbol{\lambda}_s + L_\sigma\mathbf{I}_r \tag{6}$$

$$\mathbf{V}_r = R_r\mathbf{I}_r + L_\sigma\frac{d\mathbf{I}_r}{dt} + \frac{d\boldsymbol{\lambda}_s}{dt} + j(\omega-\omega_r)\cdot(L_\sigma\mathbf{I}_r+\boldsymbol{\lambda}_s) \tag{7}$$

The phase-angle of the stator-flux space vector is usually used for the controller synchronization in the RSC [10]. The *d*-axis of the synchronous frame is fixed to the stator flux (Fig. 3) rotating at the angular speed of ω_s. Accordingly, the space vector relationship between the stationary α-β frame, the rotor *x*-*y* frame rotating at ω_r, and the synchronous *d*-*q* frame rotating at ω_s can be defined and the vector transformations between different reference frames are formulated as

$$\mathbf{F}^{dq} = \mathbf{F}^{\alpha\beta}\cdot e^{-j\theta_s} \tag{8}$$

$$\mathbf{F}^{xy} = \mathbf{F}^{dq}\cdot e^{-j(\theta_s-\theta_r)} = \mathbf{F}^{dq}\cdot e^{-j\theta_{slip}} \tag{9}$$

where **F** represents the voltage, current, or flux space vector. Using Eqs. 1 and 5, the stator active and reactive powers can be expressed in the synchronous frame as

$$\mathbf{S}_s = -\frac{3}{2}\mathbf{V}_s\cdot\hat{\mathbf{I}}_s \Rightarrow \begin{cases} P_s = 1.5\omega_s\cdot\lambda_{sd}\cdot I_{rq} \\ Q_s = 1.5\omega_s\cdot\lambda_{sd}\cdot(I_{rd}-\dfrac{\lambda_{sd}}{L_m}) \end{cases} \tag{10}$$

According to Eq. 10, the active and reactive power of the stator winding can be independently controlled by regulating the *q*- and *d*- components of the rotor current, respectively. This means that the vector control scheme adopted for the DFIG requires the state variables of I_{rd} and I_{rq} to follow the time-varying reference points. This must be achieved by implementing the appropriate current controller in the RSC.

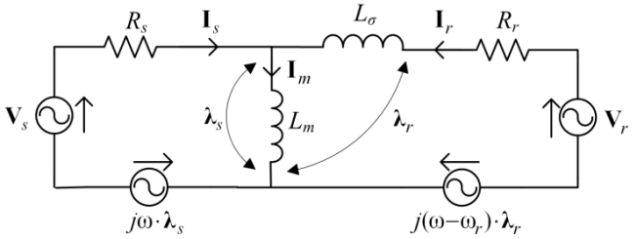

Figure2. Γ-form equivalent circuit of DFIG

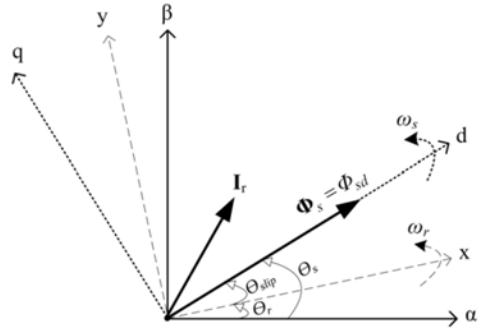

Figure 3. Vector representation of DFIG in the stator-voltage frame

III. DFIG Control System

DFIG is a standard machine controlled with a frequency converter built by two PWM converters connected through a DC link capacitor.

A. Principle of Space Vector PWM

The circuit model of a three-phase voltage source PWM inverter is shown in Fig. 4 In this model, S_1 to S_6 are the six power switches, which are controlled by the switching variables a, a′, b, b′, c and c′. When an upper transistor is switched on (i.e., when a, b or c is 1), the corresponding lower transistor is switched off (i.e., the corresponding a′, b′ or c′ is 0). Therefore, the on and off states of the upper transistors S_1, S_3 and S_5 can be used to determine the output voltage.

The relationship between the switching variable vectors (a, b, and c) and the line-to-line and phase voltage vectors are given by Eqs. 11 and 12, respectively:

$$\begin{bmatrix} V_{ab} \\ V_{bc} \\ V_{ca} \end{bmatrix} = V_{dc}\begin{bmatrix} 1 & -1 & 0 \\ 0 & 1 & -1 \\ -1 & 0 & 1 \end{bmatrix}\begin{bmatrix} a \\ b \\ c \end{bmatrix} \tag{11}$$

$$\begin{bmatrix} V_{an} \\ V_{bn} \\ V_{cn} \end{bmatrix} = \frac{V_{dc}}{3}\begin{bmatrix} 2 & -1 & -1 \\ -1 & 2 & -1 \\ -1 & -1 & 2 \end{bmatrix}\begin{bmatrix} a \\ b \\ c \end{bmatrix} \tag{12}$$

There are eight possible combinations of on and off patterns for the power switches. Based on Eqs. 11-12, the eight switching vectors, output line to neutral and line-to-line voltages in terms of DC-link V_{dc}, are given in Table I.

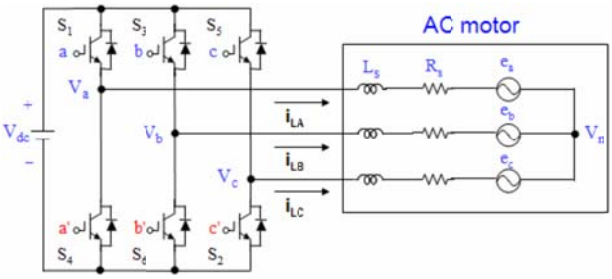

Figure 4. Three-phase volatge source PWM inverter

According to Table I, the six nonzero vectors (V_1-V_6) shape the axes of a hexagonal (Fig. 5) and feed electric power to the load. The angle between any adjacent two non-zero vectors is 60 degrees. Meanwhile, the two zero vectors (V_0 and V_7) apply zero voltage to the load. The objective of space vector PWM technique is to approximate the reference voltage vector V_{ref} using the eight switching patterns [8].

TABLE I. EIGHT INVERTER VOLTAGE VECTORS (V0-V7)

Voltage vectors	Switching Vectors			Line to Neutral Voltage			Line to Line Voltage		
	a	b	c	V_{an}	V_{bn}	V_{cn}	V_{ab}	V_{bc}	V_{ca}
V0	0	0	0	0	0	0	0	0	0
V1	1	0	0	2/3	-1/3	-1/3	1	0	-1
V2	1	1	0	1/3	1/3	-2/3	0	1	-1
V3	0	1	0	-1/3	2/3	-1/3	-1	1	0
V4	0	1	1	-2/3	1/3	1/3	-1	0	1
V5	0	0	1	-1/3	-1/3	2/3	0	-1	1
V6	1	0	1	1/3	-2/3	1/3	1	-1	0
V7	1	1	1	0	0	0	0	0	0

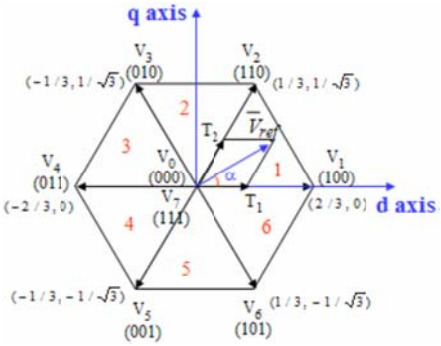

Figure 5. The basic switching vectors and sectors

B. *Control of RSC*

The first step for the control of RSC is to determine the instantaneous stator rotating flux vector location θ_s which is delivered through:

$$V_s = R_s.i_s + \frac{d\lambda_s}{d_t} \quad (13)$$

$$\lambda_{\alpha s} = \int (V_{\alpha s} - R_s.i_{\alpha s})dt, \;\; \lambda\beta s = \int (V_{\beta s} - R_s.i_{\beta s})dt \quad (14)$$

$$\lambda_s = \sqrt{\lambda_{\alpha s}^2 + \lambda_{\beta s}^2} \quad (15)$$

$$\theta_s = \tan^{-1}(\frac{\lambda_{\alpha s}}{\lambda_{\beta s}}) \quad (16)$$

The next step is to generate the rotor current references. For this purpose two PI regulators with the inputs of Q_{ref} and W_{pu} are used (Fig. 6). The rotor is rotating and is instantaneously located at angle ϕ_r while the stator's magnetic field vector is at location ϕ_s. ϕ_r, which is defined as the "slip angle" ϕ_{slip}. The instantaneous values for the desired rotor currents can then be readily calculated using the inverse dq transformation, with respect to the slip angle. Once the reference currents ($i_{a\text{-}ref}$, $i_{b\text{-}ref}$ and $i_{c\text{-}ref}$) are determined, they will be compared with the real rotor side currents and the error is be used to fire the IGBT according to the hysteresis gain h_y (Fig. 7).

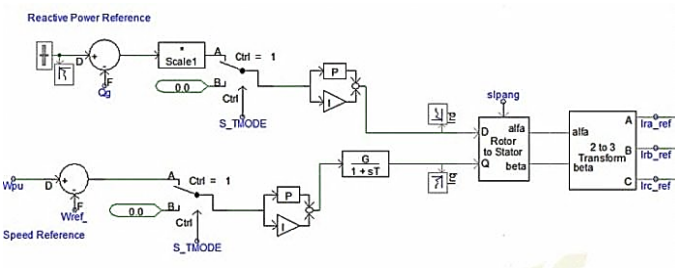

Figure 6. Generating rotor current references

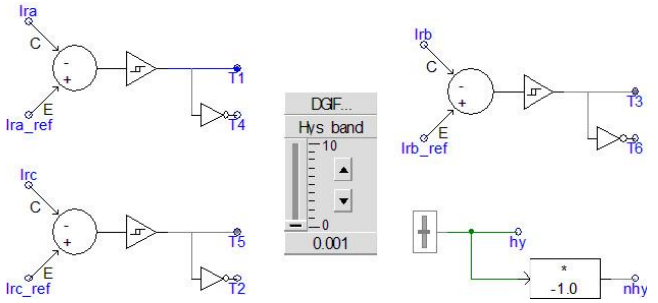

Figure 7. Hystersis control

In this control method, three hysteresis bands of width δ_{hys} are defined around each reference value of the three-phase currents. Accordingly, each phase current is controlled with a 2-level hysteresis comparator, as shown in Fig. 8a. When the line current becomes greater (or less) than the current reference as specified by the hysteresis band δ_{hys}, the respective inverter leg is switched in the negative (or positive) direction. These results in a control scheme targeted to keep the current error within the hexagonal band shown in Fig. 8b [16]. Note that in this figure the tolerance region is drawn extremely large for the sake of clarity. The hexagon centre is pointed by the command current vector at each instant, and it circulates around the origin of the coordinated α-β system with the fundamental frequency. Once the output current vector touches the hexagon surface, the current error exceeds δ_{hys} and the VSI output voltage space vector must be switched in the direction of the current error vector to force the current back into the hexagon area. Nevertheless, there is a mutual interaction between three phase currents in the case of isolated load neutral. Under this interphases dependency, when the conduction state of an inverter leg changes, the resulting voltage space vector is dependent on the states of the other two inverter legs. This causes unnecessary high switching frequency at low counter emf voltage and the actual current

error reaching twice of the permitted hysteresis band ($2\delta_{hys}$), shown by the dashed area in Fig. 8b [15].

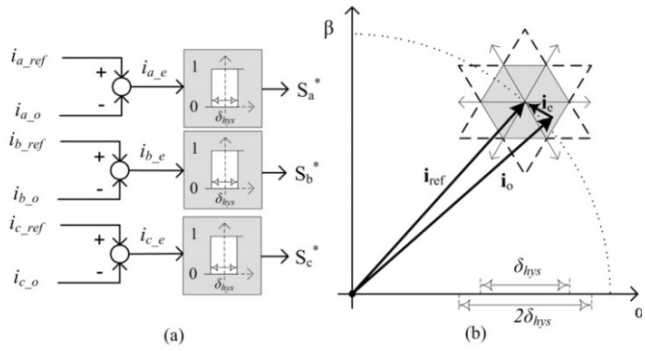

Figure 8. The conventional three-phase hysteresis method; (a) schematic diagram, (b) designated error surface

C. Control of GSC

The rotor side voltage source convertor (VSC) requires a dc power supply. The dc voltage is usually generated using another voltage sourced converter connected to the ac grid at the generator stator terminals. VSC regulates the DC bus capacitor voltage in order to keep it at a constant value and to achieve unity power factor in order to exchange reactive power through the stator. In the other words, this means that the grid side converter is supplying the real power demands of the rotor side converter. The d axis current can be controlled by the d component of SPWM while the q axis current is determined by the q component. However, any change in i_d will also cause transient variations in the i_q. Therefore, some modifications are made to the basic PI controller structure so that a decouple response of i_d and i_q can be achieved (Figs. 9-10).

A VSC with dc bus voltage is connected to the ac grid through a transformer with resistance R and inductance L.

$$\theta_s = \tan^{-1}\left(\frac{\lambda_{\alpha s}}{\lambda_{\beta s}}\right) \tag{16}$$

$$\frac{d}{dt}\begin{bmatrix} id \\ iq \end{bmatrix} = \begin{bmatrix} -\frac{R}{L} & \omega \\ -\omega & -\frac{R}{L} \end{bmatrix}\begin{bmatrix} id \\ iq \end{bmatrix} + \frac{1}{L}\begin{bmatrix} vd-ed \\ -eq \end{bmatrix} = \begin{bmatrix} -\frac{R}{L} & 0 \\ 0 & -\frac{R}{L} \end{bmatrix}\begin{bmatrix} X1 \\ X2 \end{bmatrix} \tag{17}$$

$$X1 = \frac{vd-ed}{L} + \omega id \quad X2 = -\frac{eq}{L} + \omega iq \tag{18}$$

$$ed = -LX1 + vd + \omega Lid, \quad eq = -LX2 - \omega Liq \tag{19}$$

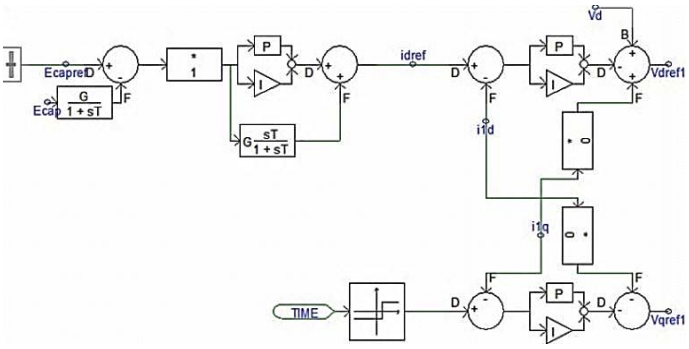

Figure 9. Grid side decoupled control

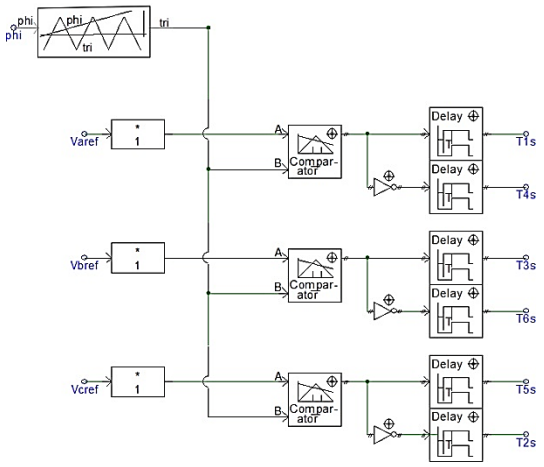

Figure 10. Grid side VSC controller

In Eq. 17, the voltage of grid is v = v_d while v_q by definition is equal to zero. This equation shows that change in i_d will cause change i_q. But by using LX1 and LX2, the resulting equations are decoupled. The schematic of decouple control of i_d and i_q is shown in Fig. 9 where the outputs are the reference voltages v_{dref1} and v_{qref1}. By converting these references to phase and magnitude and also limiting the magnitude to the maximum rating of the grid side VSC, the reference three-phase voltages are generated. Finally, each one of the phase voltages is compared with a high frequency triangle wave to determine the firing pulse patterns for grid side converter (Fig. 10).

IV. Simulation Results

A. The IEEE 14 Bus System

A single line diagram of the IEEE 14-bus system is shown in Fig. 11 [16].

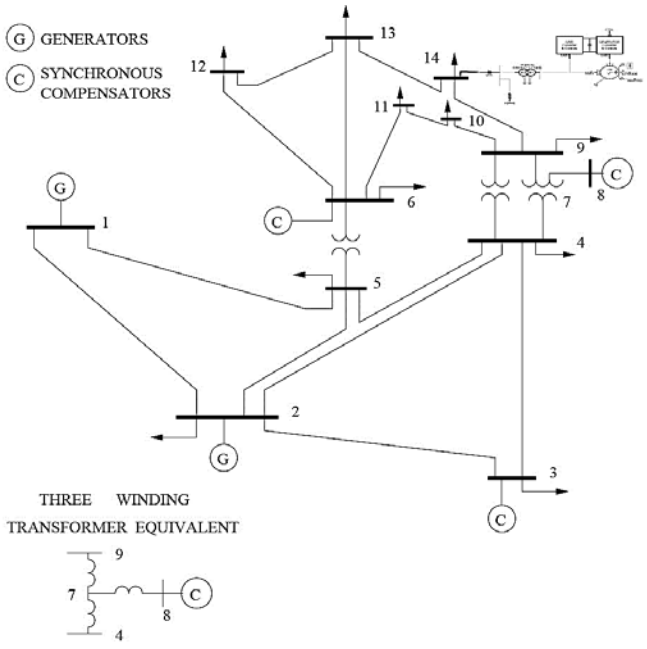

Figure 11. IEEE 14 bus system

It consists of five synchronous machines with IEEE type-1 exciters, three of which are synchronous compensators are only used for reactive power support. There are 11 loads in the system with the total active and reactive ratings of 259 MW and 81.3 MVAR, respectively. The dynamic data of the generators exciters is selected from [17].

B. Selected simulation results

The wind system is connected to the IEEE 14 bus system through a circuit breaker at bus 14. At t=0 s the circuit breaker is open and each system is feeding its related loads. At t=7 s, the circuit breaker will be closed and consequently the wind system will be connected to IEEE 14 bus system. Fig. 12 illustrates the DFIG model in PSCAD/EMTDC which includes a 15 MVA wound rotor induction generator connected to the 14 bus system through a 13.8/0.69 KV transformer and a circuit breaker. Simulation results are shown in Figs. 13-17.

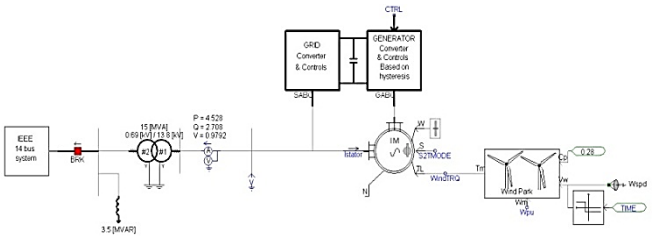

Figure 12. Simulated DFIG system in PSCAD/EMTDC

Figures 13 and 14 show the output real and reactive power of the DFIG, respectively. The output voltage of DFIG generator is shown in Fig. 15.

The voltage of all buses in the modified IEEE 14 bus system is 1 pu except for bus 14 which is around 0.94 pu (13KV). As can be seen from Fig. 16 after connection of the wind system to 14 bus system, the voltage of this bus will be improved to near 13.6 KV (0.98 pu). This shows the capability of DIFG in improving the voltage profile. Furthermore, DFIG is also participating in the control of reactive power of 14 bus system as illustrated in Fig. 17.

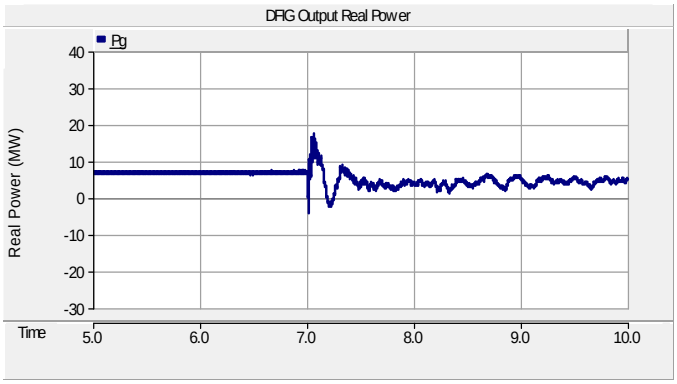

Figure 13. DFIG output real power

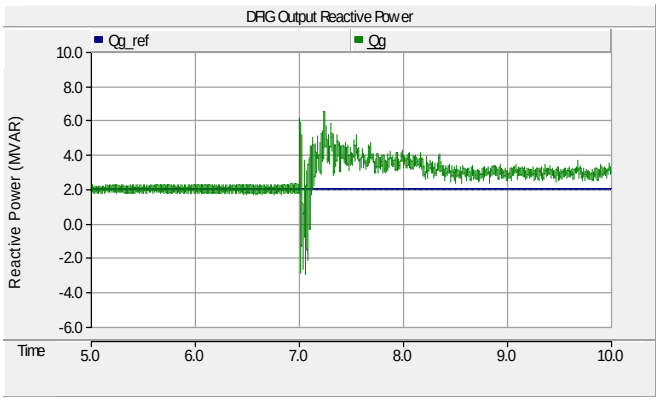

Figure 14. DFIG output reactive power

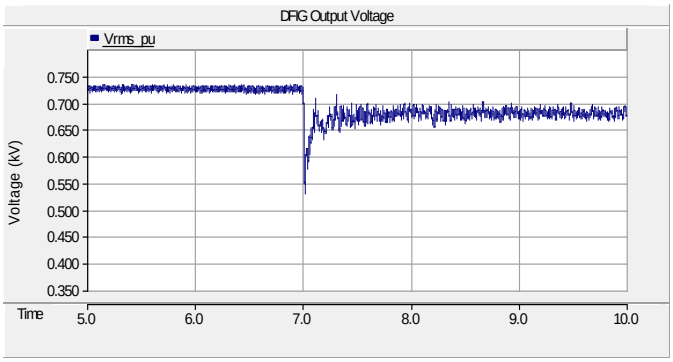

Figure 15. DFIG output voltage

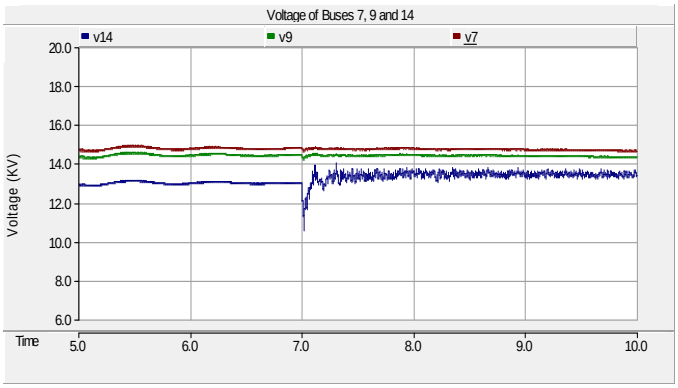

Figure 16. Voltage profiles of buses 9 and 14

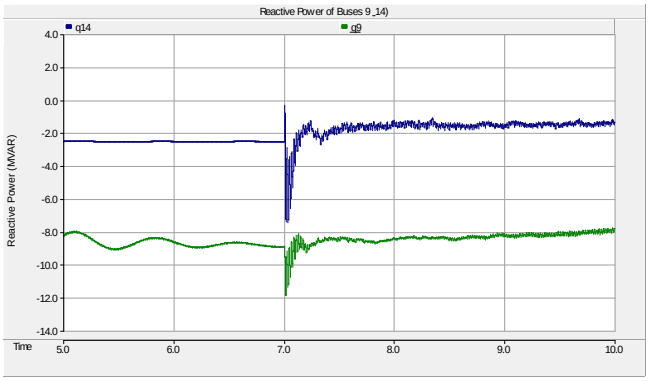

Figure 17. Reactive power of buses 9 and 14

V. CONCLUSION:

This paper examines the capability of DIFG system in providing reactive power support to the distribution system. A DIFG based wind system in simulated in PSCAD/EMTDC and connected to the IEEE 14 bus distribution system. A vector-based hysteresis current controller has been applied to DFIG control system based on the stator flux reference frame. It has shown that the DFIG system can provide reactive power to the system and also participate in regulating the system voltage profiles.

VI. REFERENCES

[1]. IEA, Wind energy annual report 2008. 2009.

[2]. J. C. Smith, "Winds of change: Issues in utility wind integration," IEEE Power Energy Mag., vol. 3, pp. 20– 25, Nov./Dec. 2005.

[3]. T. Ackermann, "Wind Power in Power Systems," Hoboken, NJ: Wiley, 2005 (ISBN: 0-470-85508-8).

[4]. A.D. Hansen, P. Sorensen, L. Janosi and J. Bech, "Wind farm modeling for power quality," Industrial Electronics Society, 2001. IECON '01. The 27th Annual Conference of the IEEE , vol.3, no., pp.1959-1964 vol.3, 2001.

[5]. M. P. Kazmierkowski and L. Malesani, "Current control techniques for three-phase voltage-source PWM converters: A survey," IEEE Trans. Ind. Electron., vol. 45, no. 5, pp. 691–703, Oct. 1998.

[6]. D.M. Brod and D.W. Novotny, "Current control of VSI-PWM inverters," IEEE Trans. Ind. Appl., vol. IA-21, no. 3, pp. 562–570, May/Jun. 1985.

[7]. S. Buso, L. Malesani, and P. Mattavelli, "Comparison of current control techniques for active filter Applications," IEEE Trans. Ind. Electron., vol. 45, no. 5, pp. 722–729, Oct. 1998.

[8]. M. Mohseni and M.Islam, "A New Vector-Based Hysteresis Current Control Scheme for Three-Phase PWM Voltage-Source Inverters" IEEE Trans. Ind. Appl., vol. 25, no. 9, pp. 2299–2309, Sep. 2010.

[9]. L. Mihet-popa, Control Strategies for large wind turbine application.

[10]. R. Pena, J. C. Clare and G. M. Asher, "Doubly fed induction generator using back-to-back PWM converters and its application to variable-speed wind-energy generation," IEEE Proc. Electr. Power Appl., vol. 143, no. 3, pp. 231–241, May 1996.

[11]. A.Tapia, G. Tapia, J. X. Ostolaza and J. R. Saenz, "Modeling and control of a wind turbine driven doubly fed induction generator," IEEE Trans. Energy Convers., vol. 18, no. 2, pp. 194–204, Jun. 2003.

[12]. S. Chondrogiannis and M. Barnes, "Stability of doubly-fed induction generator under stator voltage orientated vector control," IET Gen. Transm. Distrib., vol. 2, no. 3, pp. 170–180, 2008.

[13]. P. Vas, Vector Control of AC Machines. Oxford, U.K.: Oxford Univ. Press, 1990.

[14]. L. Xu, D. Zhi, and A.Williams, "Predictive current control of doubly fed induction generators," IEEE Trans. Ind. Electroc., Accepted for future publication.

[15]. D.M. Brod, and D.W. Novotny, "Current Control of VSI-PWM Inverters. Industry Applications," IEEE Transactions on, 1985. IA-21(3): p. 562-570.

[16]. Mithulananthan, Indices to Detect Hopf Bifurcation in Power Systems.

[17]. P.M. Anderson, "Power System Control and Stability" [Boooks and Reports]. Power Engineering Review, IEEE, 1995. 15(3): p. 40.

Moayed Moghbel (S'11) received his B.S. degree in Electrical Engineering from Khomeinishahr Azad University, Isfahan, Iran in 2003. He has four years of industrial experience in a petrochemical company as an electrical maintenance engineer and one year as a distribution project manager. He is currently working towards the master degree at Curtin University, Perth, Australia. His interests include power quality, protection and electrical machines.

Hasmina Tari Mokui (S'11) received her B.Eng in 2003 from Hasanuddin University, Makassar, Indonesia and M.E. in 2007, from University of Queensland, Brisbane, Australia, all in Electrical Engineering. She is currently working towards the PhD degree at Curtin University, Perth, Australia. Her research interests include wind power generation, grid integration of renewable energy systems, power system stability and control as well as power electronics applications on power system.

Mohammad A.S. Masoum (S'88–M'91–SM'05) received his B.S., M.S. and Ph.D. degrees in Electrical and Computer Engineering in 1983, 1985, and 1991, respectively, from the University of Colorado, Boulder, USA. His research interests include optimization, power quality and stability of power systems/electric machines and distributed generation. Dr. Masoum is the co-author of "Power Quality in Power Systems and Electrical Machines" (Elsevier, 2008) and "Power Conversion of Renewable Energy Systems" (Springer, 2011). Currently, he is an Associate Professor and the discipline leader for electrical power engineering at the Electrical and Computer Engineering Department, Curtin University, Perth, Australia and a senior member of IEEE.

Mansour Mohseni (S'09, M'11) received the B.Sc. and M.Sc. degrees in electrical power engineering from Shahid Chamran University, Ahwaz, Iran, in 2004 and 2007, respectively, and the PhD degree in electrical and computer engineering from Curtin University, Perth, Australia, in 2011. He is currently an associate lecturer at the Department of Electrical and Computer Engineering, Curtin University, Perth, Australia. He is the author or co-author of over 30 published technical papers in his area of expertise. His research interests include wind power generation, grid integration of renewable energy systems, and power electronics.